Enhanced diffusion and universal Rouse-like scaling of an active polymer in poor solvent

Suman Majumder [1,*] Subhajit Paul [2,3,†] and Wolfhard Janke [4,‡]

[1]*Amity Institute of Applied Sciences, Amity University Uttar Pradesh, Noida 201313, India*

[2]*International Center for Theoretical Sciences, Tata Institute of Fundamental Research, Bangalore-560089, India*

[3]*Department of Physics and Astrophysics, University of Delhi, Delhi 110007, India*

[4]*Institut für Theoretische Physik, Universität Leipzig, IPF 231101, 04081 Leipzig, Germany*

(Received 24 August 2023; accepted 12 June 2024; published 8 July 2024)

By means of Brownian dynamics simulations we study the steady-state dynamic properties of a flexible active polymer in a poor solvent condition. Our results show that the effective diffusion constant of the polymer $D_{\rm eff}$ gets significantly enhanced as activity increases, much like in active particles. The simulation data are in agreement with a theoretically constructed Rouse model of active polymer, demonstrating that irrespective of the strength of activity, the long-time dynamics of the polymer chain is characterized by a universal Rouse-like scaling $D_{\rm eff} \sim N^{-1}$, where N is the chain length. We argue that the presence of hydrodynamic interactions will only have an insignificant effect on the observed scaling behavior.

DOI: 10.1103/PhysRevMaterials.8.075601

I. INTRODUCTION

Biomolecules are subjected to athermal fluctuations originating from chemical reactions or other energy conversions, rendering them to fall out of equilibrium. Often that is the underlying cause for many biological activities, e.g., bacterial motion, shape fluctuations of red blood cell membranes, enzyme catalysis [1–5]. Hence, given the enormous progress in understanding of active particles [6–8], over the years a number of studies on active polymers have emerged as well [9–20]. The motivation for such studies stems from the need of introducing shape variety, flexibility, and coupling topology in active entities [21–26]. Besides, it is intriguing to check how the knowledge of polymer physics [27–29] can be deployed to understand active matters.

Active polymer models can be classified into two categories. One way is to consider the monomers as active particles and then connecting them linearly with a bond constraint [10,13,14,16,18–20]. In the other approach one takes a passive polymer, i.e., without any activity, immersed in a bath of active particles [30–35]. Apart from the biological motivation, current technical advancement allows one to synthesize polymers made of active colloids connected artificially by DNA or freely jointed droplets [36,37]. Theoretically, the constituent monomers can be made active by (i) introducing a local force tangential to the polymer backbone [13], (ii) by considering the monomers having Brownian activity [16,20], or (iii) Vicsek-like activity [17–19].

The conformations and dynamics of a passive polymer are characterized by various scaling laws [27–29]. A polymer undergoes a coil to globule transition upon changing the solvent condition from good (where monomer-solvent interaction dominates) to poor (where monomer-monomer interaction dominates). The spatial extension of the conformations, in terms of the radius of gyration R_g typically follows the scaling $R_g \sim N^{\nu}$ with respect to the chain length or number of monomers N. The values of the exponent $\nu \approx 3/5$ and $1/3$ characterize the conformations, respectively, in good and poor solvents. The dynamics of a polymer under a good solvent condition in the free-draining limit, i.e., ignoring hydrodynamics, is characterized by the Rouse scaling $D \sim N^{-1}$, where D is the diffusion constant of the center of mass of the polymer [38]. In presence of hydrodynamics, one expects the Zimm model [39] (with excluded volume interaction) to be valid exhibiting the scaling $D \sim N^{-\nu}$. In a poor solvent condition, however, there is no consensus among the available studies [40,41] with even reports of slow glassy dynamics [42].

For active polymers too, the focus has been on understanding the steady-state conformations and dynamics. Attempts have been made to adapt scaling theories of passive polymers to study active polymers in good solvent. In Ref. [13] using a local tangential active force along the polymer backbone, an activity induced collapse of a polymer in good solvent has been reported. There at large activities an enhancement of the diffusion constant was also observed, which was shown to be independent of the polymer length N for long chains. In all these previous studies the self-avoidance in good solvent condition has been realized using repulsively interacting constituent monomers. Only recently, an interaction potential with both attractive and repulsive components has been considered [16–20]. A passive polymer having such an interaction exhibits a temperature-dependent coil-globule transition. We have shown that a polymer with active Brownian monomers in poor solvent condition exhibits a transition from a globule at small activity to coil at large activity [20]. Expectedly, the dynamics of such active polymers would also reveal interesting features.

*Contact author: smajumder@amity.edu; suman.jdv@gmail.com

†Contact author: subhajit.paul@icts.res.in; spaul@physics.du.ac.in

‡Contact author: wolfhard.janke@itp.uni-leipzig.de

In this work, using computer simulation supported by analytical reasoning we investigate the steady-state dynamics of a flexible coarse-grained model active polymer in a poor solvent condition. To probe the dynamics we monitor the motions of the center of mass of the polymer and two different tagged monomers, viz., the central and end monomers. All these motions exhibit long-time diffusive behaviors allowing us to calculate the effective diffusion constant $D_{\rm eff}$ of the polymer, which shows a universal Rouse-like scaling with respect to N, at all considered strengths of activity.

The remainder of the paper is organized in the following manner. In Sec. II we present details of the model and simulation method. Followed by that in Sec. III we present our main results. Finally, in Sec. IV we provide a brief summary, conclusion, and outlook to future work.

II. MODEL AND SIMULATION METHOD

We consider a bead-spring model of a flexible polymer chain in which the monomers are connected in a linear way. The bonded interaction between successive monomers is modeled with the standard finitely extensible nonlinear elastic (FENE) potential defined as

$$V_{\rm FENE}(r) = -\frac{K}{2}R^2 \ln\left[1 - \left(\frac{r - r_0}{R}\right)^2\right], \tag{1}$$

where $K = 40$ is the spring constant, $r_0 = 0.7$ the equilibrium bond length, and $R = 0.3$ is the maximum allowed extension of the bond.

The nonbonded interaction among different monomers with separation r is modeled via the standard Lennard-Jones potential

$$V_{\rm LJ}(r) = 4\epsilon\left[\left(\frac{\sigma}{r}\right)^{12} - \left(\frac{\sigma}{r}\right)^{6}\right], \tag{2}$$

where $\epsilon = 1$ is the interaction strength. The bead diameter σ is related to r_0 as $\sigma = r_0/2^{1/6}$. This potential has a minimum at $2^{1/6}\sigma \equiv r_0$.

For computational benefit during simulations the LJ potential $V_{\rm LJ}$ is truncated and shifted at $r_c = 2.5\sigma$ such that the nonbonded interaction has the form

$$V_{\rm NB}(r) = \begin{cases} V_{\rm LJ}(r) - V_{\rm LJ}(r_c) - (r - r_c)\frac{dV_{\rm LJ}}{dr}\big|_{r=r_c} & r < r_c, \\ 0 & \text{otherwise}, \end{cases} \tag{3}$$

which has the same qualitative behavior as $V_{\rm LJ}$.

Each bead is considered as an active Brownian particle. The activity for each bead works along its intrinsic propulsion direction, which changes stochastically with time. Thus the overdamped dynamics for each bead is modeled via the equations in an implicit solvent

$$\partial_t \vec{r}_i = \frac{D_{\rm tr}}{k_B T}[f_p \hat{n}_i - \vec{\nabla} U_i] + \sqrt{2D_{\rm tr}}\,\vec{\Lambda}_i^{\rm tr}, \tag{4}$$

and

$$\partial_t \hat{n}_i = \sqrt{2D_{\rm rot}}\left(\hat{n}_i \times \vec{\Lambda}_i^{\rm rot}\right), \tag{5}$$

where $\vec{r}_i$ and $\hat{n}_i$ represent the position and orientational direction of the i-th bead, respectively, U_i is the passive interaction consisting of both $V_{\rm FENE}$ and $V_{\rm NB}$, and f_p denotes the strength of the self-propulsion force acting along $\hat{n}_i$. $\vec{\Lambda}_i^{\rm tr}$ and $\vec{\Lambda}_i^{\rm rot}$ are random noises with zero mean and unit variance and are δ-correlated over different particles and time given by

$$\left\langle \vec{\Lambda}_i(t)\vec{\Lambda}_j^T(t')\right\rangle = \mathbf{I}\delta_{ij}\delta(t, t'), \tag{6}$$

where $\mathbf{I}$ is the identity matrix. In Eqs. (4) and (5) $D_{\rm tr}$ and $D_{\rm rot}$ are the translational and rotational diffusion constants, which are related via the parameter Δ as

$$\Delta = \frac{D_{\rm tr}}{D_{\rm rot}\sigma^2}, \tag{7}$$

where we have considered $\Delta = 1/3$ in our simulations. The translational diffusion constant $D_{\rm tr}$ is related to the temperature T and the drag or friction coefficient γ as $D_{\rm tr} = k_B T/\gamma$. We have chosen $\gamma = 1$ and set the integration time step for MD simulations to 10^{-5} in units of the time scale $\tau_0 = \sigma^2\gamma/\epsilon$ ($\propto 1/D_{\rm rot} = \Delta\sigma^2\gamma/k_B T$ at fixed $k_B T/\epsilon$).

The activity is measured in terms of a dimensionless quantity, the Péclet number Pe, defined as the ratio between the active force f_p and the thermal force $k_B T/\sigma$ as

$$Pe = \frac{f_p\sigma}{k_B T}. \tag{8}$$

In our simulations we have fixed the temperature at $T = 0.1\epsilon/k_B$, well below the coil-globule or θ-transition temperature of the passive polymer (the case with $Pe = 0$), thus mimicking a poor solvent condition [43]. At the same time this temperature is small enough to keep the thermal noise much lower compared to the active force. In all the subsequent results activity is expressed in terms of Pe.

We started our simulations using self-avoiding coils as initial condition. Then, we allow the system to reach its steady state by running it for sufficiently long times at the desired T and Pe. All the presented quantities are calculated after the polymer reaches its corresponding steady state. We considered chains with N varying between $32 \leqslant N \leqslant 380$ and self-propulsion value Pe between $0 \leqslant Pe \leqslant 62.5$.

III. RESULTS

Typical steady-state conformations of a polymer of length $N = 128$ obtained for different Pe are presented in Fig. 1. The conformation of the passive polymer, i.e., $Pe = 0$, is a perfectly collapsed globule. It remains in such a globular state for relatively smaller activities $Pe \leqslant 25$ as well. For intermediate values of Pe one may observe globule or head-tail-like conformations (as the one presented for $Pe = 37.5$). For even larger Pe the polymer becomes an extended coil. The corresponding quantitative picture is presented in Fig. 1 in the form of the distribution of end-to-end distance

$$R_e = |\vec{r}_N - \vec{r}_1|. \tag{9}$$

It shows that for $Pe < 37.5$ the peaks are at $R_e \approx 3$, indicative of collapsed globules. The decrease in peak height as Pe increases is reflective of the fact that the probability of getting a collapsed globule decreases and encountering a head-tail-like conformations increases. For $Pe > 37.5$ the distribution broadens and the peak position shifts towards $R_e > 15$ suggesting a dominance of coil-like conformations. The overall picture is reminiscent of the temperature driven coil-globule

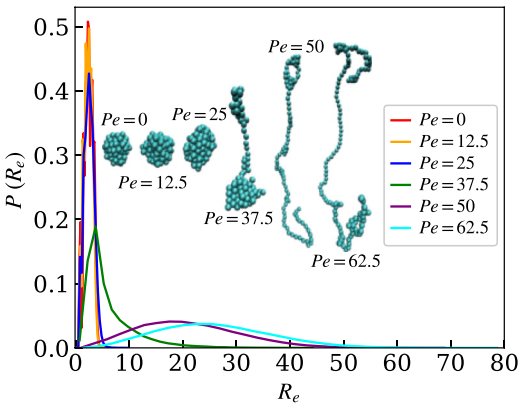

FIG. 1. Typical steady-state conformations of a polymer of length $N = 128$ at different activity strength Pe, obtained from simulations at a fixed temperature $T = 0.1\epsilon/k_B$. The plots are for corresponding normalized distributions of the end-to-end distance R_e.

transition of a passive polymer. Here, however, it is driven by the activity strength. In fact, we have confirmed in Ref. [20] that the conformations obey the scaling law $R_g \sim N^{\nu}$ with $\nu = 1/3$ and $\approx 3/5$, respectively, at small and large Pe.

To probe the dynamics we monitor the trajectory of the position vector of the center of mass (cm), central monomer or bead (cb), and end beads (eb) of the polymer given as

$$\vec{r}_{\rm cm} = \frac{1}{N}\sum_{i=1}^{N}\vec{r}_i;\ \vec{r}_{\rm cb} = \vec{r}_{N/2};\ \vec{r}_{\rm eb} = \vec{r}_1 \text{ and } \vec{r}_N. \tag{10}$$

A bare look at the typical trajectories over a fixed time period as presented in Fig. 2 reveals that although motions are random in general, the distance covered varies significantly for different Pe. From the obtained trajectories we calculate the corresponding mean-square displacements

$$\mathrm{MSD}_i(t) = \langle[\vec{r}_i(t) - \vec{r}_i(0)]^2\rangle;\ i \equiv \text{cm, cb, and eb}, \tag{11}$$

as a function of time t. Figure 3(a) shows that the cm exhibits a typical long-time diffusive motion $\sim t$, with pronounced short-time ballistic behavior as the activity increases. A similar long-time behavior is also observed for the motions of cb and eb, shown, respectively, in Figs. 3(b) and 3(c). Significantly, different is the appearance of an intermediate regime, which becomes longer as Pe increases. In this regime the behavior of the central bead appears to be $\sim t^{2/3}$ for large Pe, which may lure one to consider it as Zimm's scaling of a passive polymer in good solvent [44–47]. However, this is very unlikely since our simulations do not consider hydrodynamics. The end beads show an extended intermediate regime, although the corresponding power-law exponent seems to be smaller than $2/3$. This rather suggests a Rouse-like behavior, expected for a passive polymer in good solvent.

For a better understanding of the time-dependent power-law behavior of $\mathrm{MSD}_i \sim t^{\alpha}$, we calculate the instantaneous exponent

$$\alpha_i(t) = \frac{d\ln \mathrm{MSD}_i(t)}{d\ln t}. \tag{12}$$

Corresponding plots of $\alpha_i(t)$ are presented in Fig. 4. The exponent $\alpha_{\rm cm}$ for $Pe > 0$ starts at a value >1 and quickly [beginning of the darker shade in Fig. 4(a)] approaches 1, consistent with the long-time diffusive behavior.

For $Pe \geqslant 50$, where the polymer is in a coiled state, starting from a value around 0.9, the exponent $\alpha_{\rm cb}$ drops significantly before it climbs up in the diffusive regime [Fig. 4(b)]. However, one can hardly see a flat intermediate region to consider this as a true scaling regime. Importantly, the data never really show a steady behavior around the value $2/3$, thus ruling out the apparent Zimm's scaling. This drop in $\alpha_{\rm cb}$ can rather be interpreted as an effect of gradual crossover to the long-time diffusive regime. The crossover gets delayed with increase in Pe, as evident from Figs. 3(d)–3(f) showing that the data for $\mathrm{MSD}_{\rm cb}(t)$ merge with the one for $\mathrm{MSD}_{\rm cm}(t)$ at large t.

The time-dependent exponent $\alpha_{\rm eb}(t)$ for the end beads shows a similar behavior of approaching 1 at late times [Fig. 4(c)]. This implies that the data for $\mathrm{MSD}_{\rm eb}(t)$ must coincide with $\mathrm{MSD}_{\rm cm}(t)$ at large t, which can be verified from the plots in Figs. 3(d), 3(e), and 3(f). Similar to $\alpha_{\rm cb}$, at intermediate times the data for $\alpha_{\rm eb}$ show a drop from 1 and tend to become flat before it finally approaches 1 at large t. This indicates the presence of a true intermediate power-law regime. For $Pe \geqslant 50$, the value of $\alpha_{\rm eb}$ in the intermediate flat regime is less than $2/3$. For a Rouse polymer with excluded volume, in the intermediate regime, the scaling for the end monomers is given by [44–46,48]

$$\mathrm{MSD}_{\rm eb}(t) \sim t^{2\nu/(1+2\nu)}. \tag{13}$$

For a Gaussian chain having $\nu = 1/2$ this provides a $\sim t^{1/2}$ behavior. In the present case at large Pe, the polymer behaves like a self-avoiding coil with $\nu \approx 3/5$ producing a scaling $\sim t^{6/11}$. Our data is indeed consistent with such a behavior, shown by the dashed lines in Figs. 3(c) and 3(f). Thus it can be inferred that the intermediate Rouse scaling, which in general does not hold for a passive polymer in poor solvent [42], can be recovered in an active polymer at sufficiently large strength of activity.

To provide a theoretical understanding for the scaling behavior observed for the effective diffusion constant $D_{\rm eff}$ of cm of the active polymer in poor solvent, we consider an analog of the Rouse model [38]. For a passive polymer, the Rouse model correctly predicts the scaling of the diffusion constant in absence of hydrodynamic effects in good solvent. It is a bead-spring model where only a harmonic potential is considered to mimic the bonded interaction between successive monomers. In the active Rouse model, in addition to the above feature, we consider that the monomers are active Brownian particles, and there exists a nonbonded interaction between the monomers in order to take care of the solvent condition. For a polymer chain of length N, the equation of motion for a bead (except the ones at the ends) can be written as:

$$\dot{\vec{r}}_i = -k(2\vec{r}_i - \vec{r}_{i-1} - \vec{r}_{i+1}) + \vec{F}_i;\quad i \in [2, N-1], \tag{14}$$

where k is the spring constant of the harmonic bonds and $\vec{F}_i$ is the net force acting on the bead due to a combination of the thermal noise, self-propulsion, or active force, and the

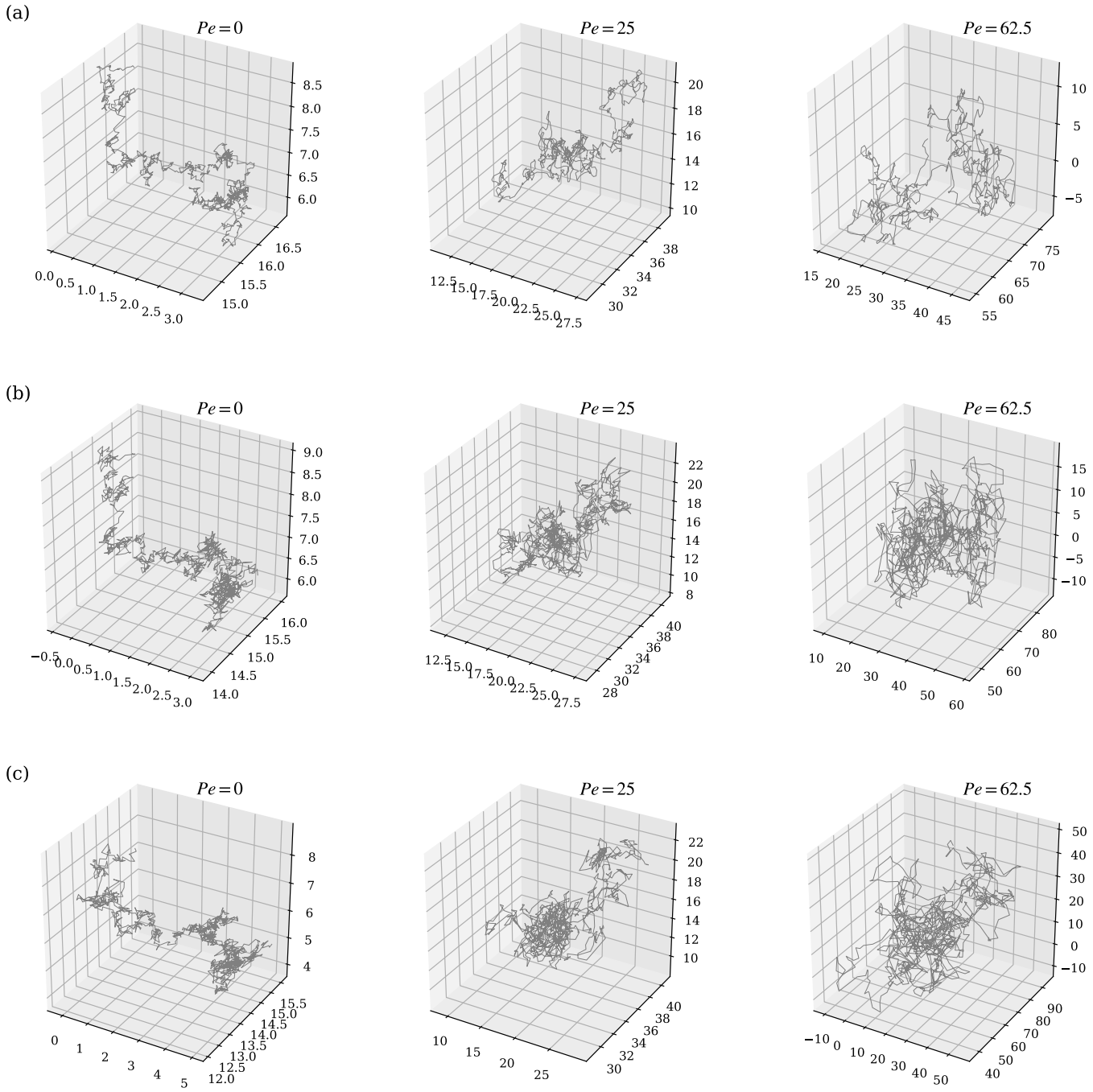

FIG. 2. Typical trajectories of the (a) center of mass, (b) central monomer, and (c) end monomer of a polymer of length $N = 128$, for different strengths of activity Pe at temperature $T = 0.1\epsilon/k_B$. Note the increasing spatial scales with increasing Pe.

nonbonded interaction in poor solvent condition. Since the end monomers experience only one bonded interaction, their equations of motion are given as

$$\dot{\vec{r}}_1 = -k(\vec{r}_1 - \vec{r}_2) + \vec{F}_1, \tag{15}$$

and

$$\dot{\vec{r}}_N = -k(\vec{r}_N - \vec{r}_{N-1}) + \vec{F}_N. \tag{16}$$

Adding (14), (15), and (16), the equation of motion of the cm of the polymer is obtained as

$$\dot{\vec{r}}_{\rm cm} = \frac{1}{N}\sum_{i=1}^{N}\vec{F}_i. \tag{17}$$

Integrating Eq. (17) we get

$$\vec{r}_{\rm cm}(t) - \vec{r}_{\rm cm}(0) = \frac{1}{N}\int_0^t dt'\left[\sum_{i=1}^{N}\vec{F}_i(t')\right]. \tag{18}$$

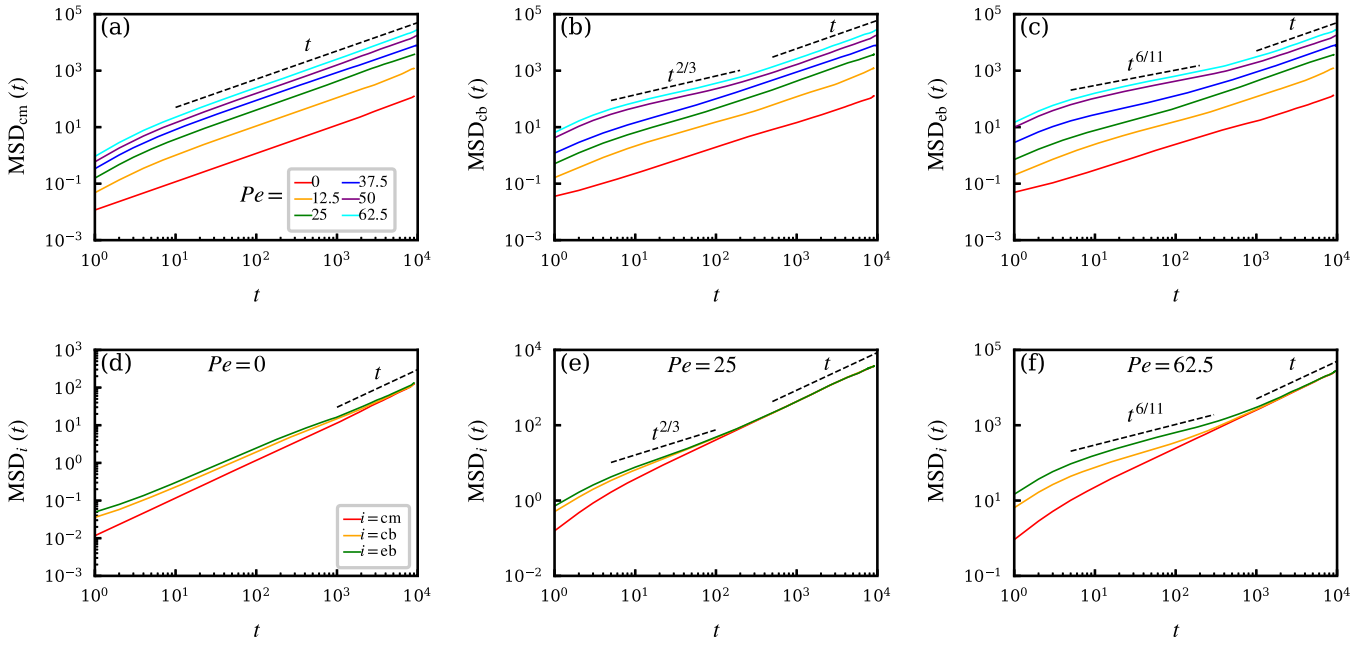

FIG. 3. Steady-state mean-square displacement $\mathrm{MSD}_i(t)$ of the (a) center of mass, (b) central bead, and (c) end beads of a polymer of length $N = 128$ for different activity strengths Pe. Plots in (d), (e), and (f) present a comparison among the different MSDs for different values of Pe. The dashed lines represent different power laws. All data are from simulations at temperature $T = 0.1\epsilon/k_B$.

This leads to the expression for MSD of the cm of the polymer as

$$\mathrm{MSD}_{\mathrm{cm}}(t) = \langle[\vec{r}_{\mathrm{cm}}(t) - \vec{r}_{\mathrm{cm}}(0)]^2\rangle = \frac{1}{N^2}\left\langle \int_0^t \int_0^t dt'dt'' \left[\sum_{i=1}^{N} \vec{F}_i(t')\right]\cdot\left[\sum_{j=1}^{N} \vec{F}_j(t'')\right]\right\rangle. \tag{19}$$

We assume that the net force $\vec{F}_i$ acting on an individual bead is random and δ-correlated over space and time, i.e.,

$$\langle \vec{F}_i(t')\vec{F}_j(t'')\rangle = 6\frac{D_{\mathrm{a}}}{D_m}\delta_{ij}\delta(t'-t''), \tag{20}$$

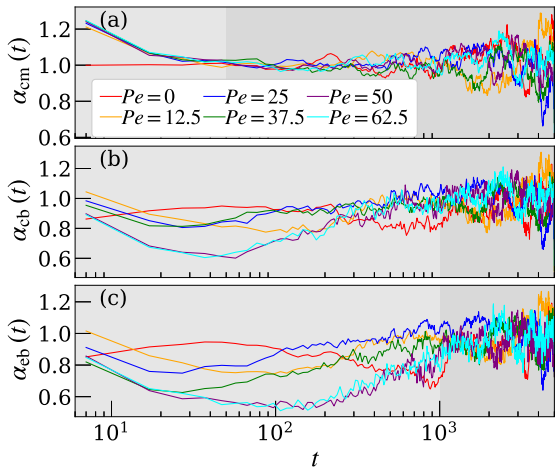

FIG. 4. Time-dependent exponent $\alpha_i(t)$ for the data presented in Fig. 3. The gray shades are introduced to distinguish the early-time regime from the long-time diffusive regime.

where D_{a} is the diffusion constant of an active particle and D_m is the factor by which D_{a} gets modified in a poor solvent condition. Thus the effective diffusion constant of the bead becomes D_{a}/D_m. Using Eq. (20) in Eq. (19) we obtain

$$\mathrm{MSD}_{\mathrm{cm}}(t) = 6D_{\mathrm{eff}}t, \tag{21}$$

where D_{eff} is the effective diffusion constant of the cm of the polymer and is given as

$$D_{\mathrm{eff}} = \frac{(D_{\mathrm{a}}/D_m)}{N}. \tag{22}$$

In Eq. (22), the expression for D_{a} can be derived from $\mathrm{MSD}(t) = 6D_{\mathrm{a}}t$ of a noninteracting active Brownian particle, which is given as [49]

$$\mathrm{MSD}_{\mathrm{a}}(t) = \langle[\vec{r}_i(t) - \vec{r}_i(0)]^2\rangle = 6D_{\mathrm{tr}}t + \frac{v_0^2}{D_{\mathrm{rot}}^2}[D_{\mathrm{rot}}t + \exp(-D_{\mathrm{rot}}t) - 1], \tag{23}$$

where D_{tr} and D_{rot} are the translational and rotational diffusion constants, respectively, as defined previously in Sec. II, and v_0 is the ballistic velocity. At large t ($\gg \tau_0$), $D_{\mathrm{rot}}t \gg 1$ and Eq. (23) reduces to

$$\mathrm{MSD}_{\mathrm{a}}(t) = \left(6D_{\mathrm{tr}} + \frac{v_0^2}{D_{\mathrm{rot}}}\right)t. \tag{24}$$

Inserting $D_{\mathrm{tr}} = k_BT/\gamma$, $D_{\mathrm{rot}} = 3D_{\mathrm{tr}}/\sigma^2$, and the ballistic velocity for each bead $v_0 = f_p/\gamma = Pek_BT/\sigma\gamma$, Eq. (24) transforms to

$$\mathrm{MSD}_{\mathrm{a}}(t) = \left(1 + \frac{Pe^2}{18}\right)\frac{6k_BTt}{\gamma}. \tag{25}$$

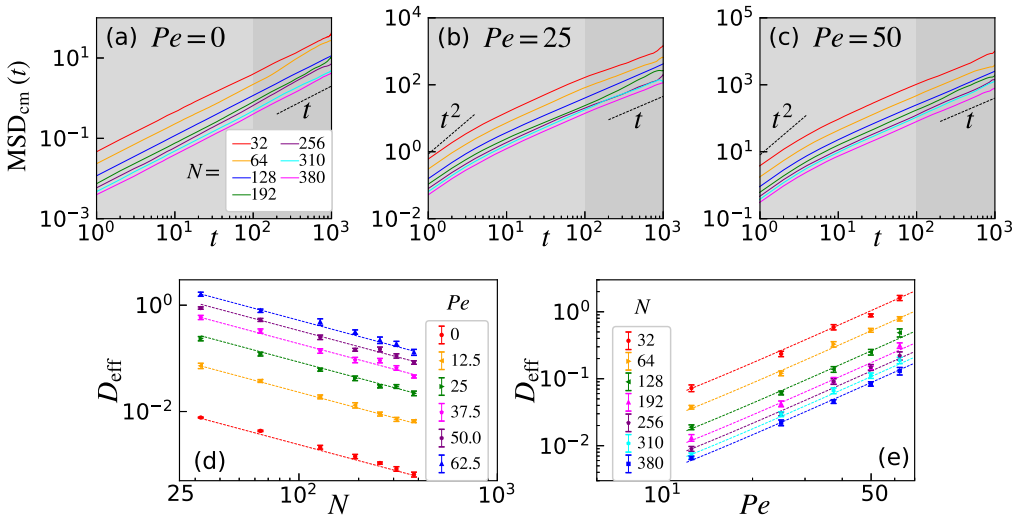

FIG. 5. Chain-length dependence of the mean-square displacement of the center of mass of the polymer at temperature $T = 0.1\epsilon/k_B$ for (a) $Pe = 0$, (b) $Pe = 25$, and (c) $Pe = 62.5$. Regions with darker shades mark the time period $t \in [10^2 : 10^3]$, over which the diffusion constant D_{eff} is calculated. (d) Scaling of D_{eff} with N for different Pe. The dashed lines represent the scaling $D_{\text{eff}} \sim N^{-1}$ for fixed Pe, predicted in Eq. (27) using $D_m = 0.42$. (e) D_{eff} as a function of Pe for different N. There the dashed lines represent the scaling $D_{\text{eff}} \sim Pe^2$ for fixed N, embedded in Eq. (27) using $D_m = 0.42$.

This provides the diffusion constant of an active particle as

$$D_{\text{a}} = \left(1 + \frac{Pe^2}{18}\right)\frac{k_B T}{\gamma}. \tag{26}$$

Finally, inserting the above expression of D_{a} in Eq. (22) we get

$$D_{\text{eff}} = \left(1 + \frac{Pe^2}{18}\right)\frac{k_B T}{\gamma D_m N}, \tag{27}$$

implying a Rouse-like scaling $D_{\text{eff}} \sim N^{-1}$ at a fixed Pe, and $D_{\text{eff}} \sim Pe^2$ for fixed N.

We now calculate

$$D_{\text{eff}} = \frac{1}{6}\lim_{t\to\infty}\frac{d}{dt}\text{MSD}_{\text{cm}}(t), \tag{28}$$

using the simulation data for $\text{MSD}_{\text{cm}}(t)$ for different N, presented in Figs. 5(a)–5(c). The extracted D_{eff} as a function of N for fixed Pe are presented in Fig. 5(d) showing a power-law scaling. Similarly, as Pe increases a significant enhancement of D_{eff} is noticed, depicted in Fig. 5(e) via plots of D_{eff} as a function of Pe for fixed N, also showing a power-law scaling. The dashed lines in Figs. 5(d) and 5(e) represent the prediction in Eq. (27) with $D_m = 0.42$, obtained following a rigorous fitting exercise presented in Appendix A. The consistency of our data with the dashed lines in Fig. 5(d) confirms the presence of a universal Rouse-like scaling with the chain length N for fixed Pe, embedded in the prediction (27). At the same time the consistency of the data with the dashed lines in Fig. 5(e) not only depict an unambiguous validity of the prediction in Eq. (27) but also indicates that the modification factor D_m is rather universal, regardless of N and Pe.

Enhanced diffusion of repulsive active particles can be understood via mapping to effectively high-temperature passive Brownian particles [50]. A similar mapping could qualitatively explain the enhanced diffusion observed here for the center-of mass of the active polymer. However, given the bond constraint between successive monomers and the attractive poor solvent condition this mapping is still open to interpretation. Even though we do not model hydrodynamic interactions in the simulations, our predictions should still hold strong for a wide range of realistic situations where hydrodynamics is negligible. Typically, in the equation of motion of the active monomers one can include hydrodynamic tensors without affecting the activity term [14,51,52]. This is justified by the rational that the beads are intrinsically self-propelled, independent of the external conditions including the solvent effects [9]. With such a setup it can be argued that apart from a small window in the low-activity limit, it is very unlikely that hydrodynamic interactions are going to change the scaling behaviors observed here (see Appendix B).

IV. CONCLUSION

In conclusion, this work explores the steady-state dynamics of an active Brownian polymer in poor solvent. We have investigated the dynamics by monitoring the motions of the center of mass, the central monomer, and the end monomers. Although they show different dynamics at intermediate times as a function of activity, in the long-time limit the mean-square displacement of the central and end monomers merge with the diffusive behavior of the center of mass, allowing us to estimate an effective diffusion constant D_{eff} of the polymer. Analytically, we predict an enhanced diffusion of the polymer obeying the scalings $D_{\text{eff}} \sim N^{-1}$ and $D_{\text{eff}} \sim Pe^2$ as a function of the chain length N and activity strength Pe, respectively. Our numerical results are in perfect agreement with the theoretical predictions. Furthermore, we have argued that hydrodynamic interactions should not influence the scaling behavior observed here. However, still it would be worth to explore explicit solvent simulations of this apparently universal dynamics of active polymers [53–55].

As another future endeavour, it would be rewarding to perform similar investigations of other active polymer models.

Our result of activity induced enhanced diffusion of a polymer in a poor solvent condition might indulge in design of synthetic active polymers, which potentially can be employed in delivering drugs for a wide variety of medium. It would also be interesting to explore the robustness of the observed scalings for semiflexible polymers with activity [56].

ACKNOWLEDGMENTS

This work was funded by the Deutsche Forschungsgemeinschaft (DFG, German Research Foundation) under Grant No. 189 853 844–SFB/TRR 102 (Project B04) and further supported by the Deutsch-Französische Hochschule (DFH-UFA) through the Doctoral College "$\mathbb{L}^4$" under Grant No. CDFA-02-07, and the Leipzig Graduate School of Natural Sciences "BuildMoNa". S.M. thanks the Science and Engineering Research Board (SERB), Govt. of India for funding through a Ramanujan Fellowship (File No. RJF/2021/000044). S.P. acknowledges ICTS-TIFR, DAE, Govt. of India for a research fellowship under Project No. RTI4001.

APPENDIX A: FITTING RESULTS

Equation (27) predicts the scaling laws $D_{\rm eff} \sim N^{-1}$ and $D_{\rm eff} \sim Pe^2$ for fixed Pe and N, respectively. In order to verify the simulation data, however, one can assume that $D_{\rm eff} \sim N^{-x}$ and $D_{\rm eff} \sim Pe^y$ for fixed Pe and N, respectively. Keeping Eq. (27) in mind, thus the ansatz for fitting can be written as

$$D_{\rm eff} = \left(1 + \frac{Pe^y}{18}\right)\frac{k_BT}{\gamma D_m N^x}. \tag{A1}$$

In Tables I–IV we tabulate the results from our fitting exercise using the above ansatz for our simulation data of $D_{\rm eff}$, both as a function of N and Pe.

From the presented fitting exercise we conclude that our simulation data is consistent with the prediction (27) using a Rouse model of active polymer. It also indicates that the only free parameter in the model $D_m \approx 0.42$ appears to be robust, independent of the chain length N and strength of activity Pe.

APPENDIX B: POSSIBLE EFFECT OF HYDRODYNAMICS

For a better comparison with an experimental situation where polymers are generally in solution, the role of hydrodynamic interaction due to the solvent should be taken into account. With this in hindsight, here we are going to argue that with the introduction of hydrodynamics interactions in the present case no significant effects are expected as far as the scaling of $D_{\rm eff}$ with N and Pe is concerned. One way of inclusion of hydrodynamic interaction is by writing the equation of motion for the active monomers as [9]

$$\partial_t \vec{r}_i = \frac{D_{\rm tr}}{k_BT} f_p \hat{n}_i - \sum_{j=1}^{N} \mathbf{H}_{ij}\vec{\nabla}U_i + \sqrt{2D_{\rm tr}}\gamma \sum_{j=1}^{N} \mathbf{H}_{ij}\vec{\Lambda}_i^{\rm tr}, \tag{B1}$$

and

$$\partial_t \hat{n}_i = \sqrt{2D_{\rm rot}}\left(\hat{n}_i \times \vec{\Lambda}_i^{\rm rot}\right), \tag{B2}$$

where

$$\left\langle \vec{\Lambda}_i^{\rm tr}(t)\vec{\Lambda}_j^{{\rm tr}^T}(t')\right\rangle = \left(\frac{D_{\rm tr}}{k_BT}\right)\mathbf{H}_{ij}^{-1}\delta(t,t'). \tag{B3}$$

The tensor $\mathbf{H}_{ij}$ is given as

$$\mathbf{H}_{ij}(\vec{r}_{ij}) = \delta_{ij}\mathbf{I}/\gamma + (1-\delta_{ij})\mathbf{\Omega}_{ij}(\vec{r}_{ij}), \tag{B4}$$

where $\mathbf{\Omega}_{ij}(\vec{r}_{ij})$ takes care of the hydrodynamic interaction arising from the interaction of the solvent molecules with the monomers. Numerically this is achieved using the Rotne-Prager-Yamakawa tensor for spherical particles [51,52] and analytically via the preaveraged Oseen tensor [28]. In the nonhydrodynamic limit $\mathbf{\Omega}_{ij}(\vec{r}_{ij}) = 0$, leading to the recovery of the equation of motions we have used in our simulations. In such a treatment the hydrodynamic interaction does not affect the activity term, which is justified by the rational that

TABLE I. Fitting results for different fixed Pe using $y = 2$ in the ansatz (A1) with both D_m and x as fit parameters. The quality of the fitting can be judged from the reduced chi-squared $\chi_r^2 = \chi^2/{\rm d.o.f}$; where d.o.f is the number of degrees of freedom. From the results we conclude that the mean values of D_m and x are 0.47 and 0.98, respectively. The corresponding standard deviations are 0.07 and 0.03, respectively.

Pe	D_m	x	χ_r^2
0.0	0.46(4)	0.96(2)	1.45
12.5	0.41(8)	1.00(4)	0.40
25.0	0.55(8)	0.96(3)	0.52
37.5	0.37(7)	1.02(4)	1.58
50.0	0.54(8)	0.96(3)	2.17
62.5	0.49(8)	0.96(5)	0.69

TABLE II. Results from fitting for different fixed Pe using $y = 2$ in the ansatz (A1) with D_m as the only fit parameter and fixing the exponent $x = 1$. The obtained mean value of D_m is 0.42 with a standard deviation of 0.03.

Pe	D_m	χ_r^2
0.0	0.39(4)	2.17
12.5	0.41(1)	0.33
25.0	0.45(8)	0.64
37.5	0.42(7)	1.37
50.0	0.46(8)	2.13
62.5	0.40(8)	0.74

TABLE III. Fitting results for different fixed N using $x = 1$ in the ansatz (A1) with both D_m and y as fit parameters. The obtained mean values of D_m and y are 0.39 and 1.97, respectively. The corresponding standard deviations are 0.04 and 0.03, respectively.

N	D_m	y	χ_r^2
32	0.47(4)	2.00(2)	1.19
64	0.40(2)	1.98(2)	0.84
128	0.35(3)	1.94(3)	0.98
192	0.37(3)	1.94(2)	2.08
256	0.35(2)	1.95(2)	2.94
310	0.40(3)	2.00(2)	0.51
380	0.37(3)	1.96(2)	0.45

TABLE IV. Results from fitting for different fixed N using $x = 1$ in the ansatz (A1) with D_m as the only fit parameter and fixing the exponent $y = 2$. The obtained mean value of D_m is 0.42 with a standard deviation of 0.03.

N	D_m	χ_r^2
32	0.47(2)	0.96
64	0.41(1)	0.77
128	0.42(2)	1.50
192	0.44(2)	2.80
256	0.40(3)	3.11
310	0.40(2)	0.41
380	0.42(1)	0.97

the origin of active force is solely due to certain intrinsic kicks that the monomers receive internally, independent of the external conditions including the effect of solvents [9]. Using the above equations it can be shown that the center of mass mean-square displacement is given as [14]

$$\mathrm{MSD}_{\mathrm{cm}}(t) = \frac{6k_BT}{N\sigma}H_{00}t + \frac{v_0^2}{D_{\mathrm{rot}}N}t. \tag{B5}$$

Here H_{00} is the zeroth mode representation of the hydrodynamic tensor $\mathbf{H}_{ij}(\vec{r}_{ij})$, which is related to the corresponding preaveraged Oseen tensor as

$$H_{nm} = \left(\frac{\sigma}{\gamma}\delta_{nm} + \Omega_{nm}\right). \tag{B6}$$

Rewriting Eq. (B5) in terms of the Péclet number Pe, it reads as

$$\mathrm{MSD}_{\mathrm{cm}}(t) \sim \frac{6k_BT}{N\sigma}H_{00}t + \frac{k_BT}{3N\gamma}Pe^2t, \tag{B7}$$

since $v_0 = Pek_BT/\sigma\gamma$. This implies that the effective diffusion constant would be

$$D_{\mathrm{eff}} \sim \left(\frac{\gamma}{\sigma}H_{00} + \frac{Pe^2}{18}\right)\frac{k_BT}{\gamma D_m N}. \tag{B8}$$

In the nonhydrodynamic limit when $H_{00} = \sigma/\gamma$, Eq. (B8) is analogous to Eq. (27) of the main text. It also implies that the scaling $D_{\mathrm{eff}} \sim Pe^2$ remains unaffected even in presence of hydrodynamics, suggesting that the quadratic dependence of the diffusion constant on the activity is rather universal. Presence of hydrodynamics may introduce an additional $\sim N^{-x}$ dependence from the first term, i.e., $H_{00}k_BT/\sigma D_m N$ in Eq. (B8) resulting in an overall dependence as

$$D_{\mathrm{eff}} = f(N^{-x}) + g(N^{-1}). \tag{B9}$$

The function f can be intuitively obtained by considering the Zimm scaling $\sim N^{-\nu}$, i.e., $\sim N^{-3/5}$ for a passive polymer in presence of hydrodynamics [39], resulting in

$$D_{\mathrm{eff}} = f(N^{-3/5}) + g(N^{-1}). \tag{B10}$$

The effective scaling of D_{eff} with respect to the polymer length N will thus depend on the relative strength of hydrodynamic interactions and the activity. In the limit of large Pe, the relevant regime for biological systems [8], the scaling will again be predominantly given by $D_{\mathrm{eff}} \sim N^{-1}$, i.e., a Rouse-like behavior. Thus we argue that apart from a small window in the low-activity limit, it is very unlikely that hydrodynamic interactions are going to change the scaling behaviors reported in the main text.

[1] X.-L. Wu and A. Libchaber, Particle diffusion in a quasi-two-dimensional bacterial bath, Phys. Rev. Lett. **84**, 3017 (2000).

[2] Y. K. Park, C. A. Best, K. Badizadegan, R. R. Dasari, M. S. Feld, T. Kuriabova, M. L. Henle, A. J. Levine, and G. Popescu, Measurement of red blood cell mechanics during morphological changes, Proc. Natl. Acad. Sci. USA **107**, 6731 (2010).

[3] E. Ben-Isaac, Y. K. Park, G. Popescu, F. L. H. Brown, N. S. Gov, and Y. Shokef, Effective temperature of red-blood-cell membrane fluctuations, Phys. Rev. Lett. **106**, 238103 (2011).

[4] A.-Y. Jee, Y.-K. Cho, S. Granick, and T. Tlusty, Catalytic enzymes are active matter, Proc. Nat. Acad. Sci. USA **115**, E10812 (2018).

[5] A.-Y. Jee, S. Dutta, Y.-K. Cho, T. Tlusty, and S. Granick, Enzyme leaps fuel antichemotaxis, Proc. Natl. Acad. Sci. USA **115**, 14 (2018).

[6] S. Ramaswamy, The mechanics and statistics of active matter, Annu. Rev. Condens. Matter Phys. **1**, 323 (2010).

[7] M. R. Shaebani, A. Wysocki, R. G. Winkler, G. Gompper, and H. Rieger, Computational models for active matter, Nature Rev. Phys. **2**, 181 (2020).

[8] J. Elgeti, R. G. Winkler, and G. Gompper, Physics of microswimmers–single particle motion and collective behavior: A review, Rep. Prog. Phys. **78**, 056601 (2015).

[9] R. G. Winkler and G. Gompper, The physics of active polymers and filaments, J. Chem. Phys. **153**, 040901 (2020).

[10] A. Kaiser, S. Babel, B. ten Hagen, C. von Ferber, and H. Löwen, How does a flexible chain of active particles swell? J. Chem. Phys. **142**, 124905 (2015).

[11] R. E. Isele-Holder, J. Elgeti, and G. Gompper, Self-propelled worm-like filaments: spontaneous spiral formation, structure, and dynamics, Soft Matter **11**, 7181 (2015).

[12] R. E. Isele-Holder, J. Jäger, G. Saggiorato, J. Elgeti, and G. Gompper, Dynamics of self-propelled filaments pushing a load, Soft Matter **12**, 8495 (2016).

[13] V. Bianco, E. Locatelli, and P. Malgaretti, Globulelike conformation and enhanced diffusion of active polymers, Phys. Rev. Lett. **121**, 217802 (2018).

[14] A. Martín-Gómez, T. Eisenstecken, G. Gompper, and R. G. Winkler, Active Brownian filaments with hydrodynamic interactions: Conformations and dynamics, Soft Matter **15**, 3957 (2019).

[15] E. Locatelli, V. Bianco, and P. Malgaretti, Activity-induced collapse and arrest of active polymer rings, Phys. Rev. Lett. **126**, 097801 (2021).

[16] S. Das, N. Kennedy, and A. Cacciuto, The coil–globule transition in self-avoiding active polymers, Soft Matter **17**, 160 (2021).

[17] S. Paul, S. Majumder, and W. Janke, Motion of a polymer globule with Vicsek-like activity: From super-diffusive to ballistic behavior, Soft Mater. **19**, 306 (2021).

[18] S. Paul, S. Majumder, S. K. Das, and W. Janke, Effects of alignment activity on the collapse kinetics of a flexible polymer, Soft Matter **18**, 1978 (2022).

[19] S. Paul, S. Majumder, and W. Janke, Role of temperature and alignment activity on kinetics of coil-globule transition of a flexible polymer, J. Phys.: Conf. Ser. **2207**, 012027 (2022).

[20] S. Paul, S. Majumder, and W. Janke, Activity mediated globule to coil transition of a flexible polymer in a poor solvent, Soft Matter **18**, 6392 (2022).

[21] W. F. Paxton, K. C. Kistler, C. C. Olmeda, A. Sen, S. K. St. Angelo, Y. Cao, T. E. Mallouk, P. E. Lammert, and V. H. Crespi, Catalytic nanomotors: Autonomous movement of striped nanorods, J. Am. Chem. Soc. **126**, 13424 (2004).

[22] S. Sanchez, A. A. Solovev, S. M. Harazim, and O. G. Schmidt, Microbots swimming in the flowing streams of microfluidic channels, J. Am. Chem. Soc. **133**, 701 (2011).

[23] S. Ebbens, M.-H. Tu, J. R. Howse, and R. Golestanian, Size dependence of the propulsion velocity for catalytic Janus-sphere swimmers, Phys. Rev. E **85**, 020401(R) (2012).

[24] I. Buttinoni, J. Bialké, F. Kümmel, H. Löwen, C. Bechinger, and T. Speck, Dynamical clustering and phase separation in suspensions of self-propelled colloidal particles, Phys. Rev. Lett. **110**, 238301 (2013).

[25] F. Kümmel, B. ten Hagen, R. Wittkowski, I. Buttinoni, R. Eichhorn, G. Volpe, H. Löwen, and C. Bechinger, Circular motion of asymmetric self-propelling particles, Phys. Rev. Lett. **110**, 198302 (2013).

[26] A. Zöttl and H. Stark, Hydrodynamics determines collective motion and phase behavior of active colloids in quasi-two-dimensional confinement, Phys. Rev. Lett. **112**, 118101 (2014).

[27] P.-G. De Gennes, *Scaling Concepts in Polymer Physics* (Cornell University Press, Ithaca, 1979).

[28] M. Doi, *Introduction to Polymer Physics* (Oxford University Press, New York, 1996).

[29] M. Rubinstein and R. H. Colby, *Polymer Physics* (Oxford University Press, New York, 2003).

[30] J. Harder, C. Valeriani, and A. Cacciuto, Activity-induced collapse and reexpansion of rigid polymers, Phys. Rev. E **90**, 062312 (2014).

[31] A. Kaiser and H. Löwen, Unusual swelling of a polymer in a bacterial bath, J. Chem. Phys. **141**, 044903 (2014).

[32] S. Chaki and R. Chakrabarti, Enhanced diffusion, swelling, and slow reconfiguration of a single chain in non-Gaussian active bath, J. Chem. Phys. **150**, 094902 (2019).

[33] X. Liu, H. Jiang, and Z. Hou, Configuration dynamics of a flexible polymer chain in a bath of chiral active particles, J. Chem. Phys. **151**, 174904 (2019).

[34] C. J. Anderson, G. Briand, O. Dauchot, and A. Fernández-Nieves, Polymer-chain configurations in active and passive baths, Phys. Rev. E **106**, 064606 (2022).

[35] K. Goswami, S. Chaki, and R. Chakrabarti, Reconfiguration, swelling and tagged monomer dynamics of a single polymer chain in Gaussian and non-Gaussian active baths, J. Phys. A: Math. Theor. **55**, 423002 (2022).

[36] B. Biswas, R. K. Manna, A. Laskar, P. B. S. Kumar, R. Adhikari, and G. Kumaraswamy, Linking catalyst-coated isotropic colloids into "active" flexible chains enhances their diffusivity, ACS Nano **11**, 10025 (2017).

[37] A. McMullen, M. Holmes-Cerfon, F. Sciortino, A. Y. Grosberg, and J. Brujic, Freely jointed polymers made of droplets, Phys. Rev. Lett. **121**, 138002 (2018).

[38] P. E. Rouse, Jr., A theory of the linear viscoelastic properties of dilute solutions of coiling polymers, J. Chem. Phys. **21**, 1272 (1953).

[39] B. H. Zimm, Dynamics of polymer molecules in dilute solution: Viscoelasticity, flow birefringence and dielectric loss, J. Chem. Phys. **24**, 269 (1956).

[40] J. Naghizadeh and J. Kovac, Cubic-lattice simulation of the dynamics of a collapsed polymer chain, Phys. Rev. Lett. **59**, 1710 (1987).

[41] A. Milchev, W. Paul, and K. Binder, Off-lattice Monte Carlo simulation of dilute and concentrated polymer solutions under theta conditions, J. Chem. Phys. **99**, 4786 (1993).

[42] A. Milchev and K. Binder, Anomalous diffusion and relaxation of collapsed polymer chains, Europhys. Lett. **26**, 671 (1994).

[43] S. Majumder, J. Zierenberg, and W. Janke, Kinetics of polymer collapse: Effect of temperature on cluster growth and aging, Soft Matter **13**, 1276 (2017).

[44] W. Paul, K. Binder, D. W. Heermann, and K. Kremer, Dynamics of polymer solutions and melts. Reptation predictions and scaling of relaxation times, J. Chem. Phys. **95**, 7726 (1991).

[45] B. Dünweg and K. Kremer, Microscopic verification of dynamic scaling in dilute polymer solutions: A molecular-dynamics simulation, Phys. Rev. Lett. **66**, 2996 (1991).

[46] B. Dünweg and K. Kremer, Molecular dynamics simulation of a polymer chain in solution, J. Chem. Phys. **99**, 6983 (1993).

[47] M. Hinczewski, X. Schlagberger, M. Rubinstein, O. Krichevsky, and R. R. Netz, End-monomer dynamics in semiflexible polymers, Macromolecules **42**, 860 (2009).

[48] R. Shusterman, S. Alon, T. Gavrinyov, and O. Krichevsky, Monomer dynamics in double-and single-stranded DNA polymers, Phys. Rev. Lett. **92**, 048303 (2004).

[49] J. R. Howse, R. A. L. Jones, A. J. Ryan, T. Gough, R. Vafabakhsh, and R. Golestanian, Self-motile colloidal particles: From directed propulsion to random walk, Phys. Rev. Lett. **99**, 048102 (2007).

[50] M. E. Cates and J. Tailleur, Motility-induced phase separation, Annu. Rev. Condens. Matter Phys. **6**, 219 (2015).

[51] J. Rotne and S. Prager, Variational treatment of hydrodynamic interaction in polymers, J. Chem. Phys. **50**, 4831 (1969).

[52] H. Yamakawa, Transport properties of polymer chains in dilute solution: Hydrodynamic interaction, J. Chem. Phys. **53**, 436 (1970).

[53] S. Majumder, H. Christiansen, and W. Janke, Dissipative dynamics of a single polymer in solution: A Lowe-Andersen approach, J. Phys.: Conf. Ser. **1163**, 012072 (2019).

[54] A. Bera, S. Sahoo, S. Thakur, and S. K. Das, Active particles in explicit solvent: Dynamics of clustering for alignment interaction, Phys. Rev. E **105**, 014606 (2022).

[55] S. Majumder, H. Christiansen, and W. Janke, Temperature and solvent viscosity tune the intermediates during the collapse of a polymer, arXiv:2405.04813.

[56] S. Majumder, S. Paul, and W. Janke (unpublished).